Shock Hugoniot of H$_2$O ice

Sarah T. Stewart[1] and Thomas J. Ahrens

Lindhurst Laboratory of Experimental Geophysics, California Institute of Technology, Pasadena, California, USA

[1] The outcome of impacts onto and between icy planetary bodies is controlled by the material response defined by the shock Hugoniot. New Lagrangian shock wave profile measurements in H$_2$O ice at initial temperatures (T_0) of 100 K, together with previous T_0 = 263 K data, define five distinct regions on the ice Hugoniot: elastic shocks in ice Ih, ice Ih deformation shocks, and shock transformation to ices VI, VII and liquid water. The critical pressures required to induce incipient melting (0.6, 4.5 GPa) and complete melting (3.7, >5.5 GPa) upon isentropic release from the shock state (for T_0 = 263, 100 K) were revised using calculated shock temperatures and entropy. On account of the >40% density increase upon transformation from ice Ih to ices VI and VII, the critical shock pressures required for melting are factors of 2 to 5 lower than earlier predicted. Consequently, hypervelocity impact cratering on planetary surfaces and mutual collisions between porous cometesimals will result in abundant shock-induced melting throughout the solar system. *INDEX TERMS:* 3944 Mineral Physics: Shock wave experiments; 3919 Equations of state; 5420 Planetology: Solid Surface Planets: Impact phenomena (includes cratering); 5460 Physical properties of materials; 6020 Comets and Small Bodies: Ice. **Citation:** Stewart, S. T., and T. J. Ahrens, Shock Hugoniot of H$_2$O ice, *Geophys. Res. Lett.*, *30*(6), 1332, doi:10.1029/2002GL016789, 2003.

1. Introduction

[2] Knowledge of the dynamic response of planetary minerals such as H$_2$O ice is required to model and interpret mutual collisions and impact cratering on icy surfaces in the solar system. The Hugoniot of H$_2$O ice describes the dynamic strength and possible shock-compressed states, which determine the mechanical and thermodynamic work done during an impact event. Previous studies of the shock properties of ice, centered at 263 K and focused on terrestrial applications, have had difficulty identifying the onset of shock-induced transformations to high-pressure phases and yielded conflicting explanations of the dynamic yield mechanism [*Gaffney*, 1985, and references therein]. Because ices on most planetary surfaces exist at ambient temperatures much below 263 K (e.g., around 200 K on Mars to around 40 K on Pluto), we conducted a detailed study of the shock response of the most common low-pressure phase, ice Ih, at 100 K to measure the temperature effect on dynamic strength and derive a new ice Hugoniot that is applicable throughout most of the solar system.

[1]Now at Geophysical Laboratory, Carnegie Institution of Washington, Washington, D.C., USA.

2. Experimental Method

[3] Shock wave profiles, representing Lagrangian particle velocity vs. time (Figure 1a), were integrated to yield shock states (stress and volume, Figure 1b) and measure dynamic strength [*Fowles and Williams*, 1970; *Larson*, 1984]. Target assemblies consisted of three or four electromagnetic gauges (64-μm thick Kapton-insulated copper film with 9 × 4 mm active area, Dynasen, Inc., Goleta, CA) placed between 3-mm thick sample discs of clear ice (Carving Ice, Anaheim, CA) (Figure 2). The density of the 50-mm diameter discs, determined from their dimensions and mass, was 932 (±19) kg m^{-3} at 100 K. Once the ice was cooled to 100 K (measured with two embedded chromel-alumel thermocouples) by liquid nitrogen spray, the target tank was evacuated to pressures of 25–55 Pa. Placed within a 2 × 2 × 2 cm^3 volume planar magnetic field produced from four 122-milliTesla NdFeB permanent magnets, the targets were impacted by planar 40-mm diameter polycarbonate projectiles (average density 1.19 g cm^{-3}), launched via compressed air or propellant gas. The impact-induced particle motion generated voltage across the gauges, which were recorded with 2 ns resolution digital oscilloscopes. The measured particle velocities were within 2% of the standard impedance-match solution [*Ahrens*, 1987] derived from the polycarbonate Hugoniot [*Marsh*, 1980].

3. Results

[4] The wave profiles record two- and three-wave shock fronts (Figure 1) which, when converted to stress-volume (σ-V) loading paths, reveal the transient states achieved before the final shock state (Figure 3). When multiple shock fronts are present, the first wave arrival is always the elastic shock, with a principal stress commonly called the Hugoniot Elastic Limit (HEL). In the experiment record presented in Figures 1a and 1b, particle velocities, u_p, of 155 m s^{-1} correspond to a HEL of 0.53 GPa (mean values of u_p and σ reported throughout).

[5] Ice Ih does not have a uniquely valued HEL. Rather, the elastic shock maximum stress supported before dynamic yielding, σ_E, depends on the initial ice temperature, T_0, and final shock pressure, P_S, (Figures 1 and 3) and is given by

$$\sigma_E(\text{GPa}) = \begin{cases} 0.398(\pm0.029) + 0.039(\pm0.012)P_S, & \text{at } T_0 \sim 100\text{K} \\ 0.161(\pm0.010) + 0.035(\pm0.007)P_S, & \text{at } T_0 \sim 263\text{K}. \end{cases}$$

The dependence of σ_E on both T_0 and P_S clarifies previous disagreements as to whether the (highly scattered) HEL data represented the onset of melting [*Larson*, 1984] or shear failure [*Gaffney*, 1985]. Because the average HEL of 263 K ice (σ_E = 0.2 GPa) was close to the ice Ih-liquid boundary, *Larson* [1984] concluded (we believe erroneously) that the HEL was related to initiation of melting within the shock
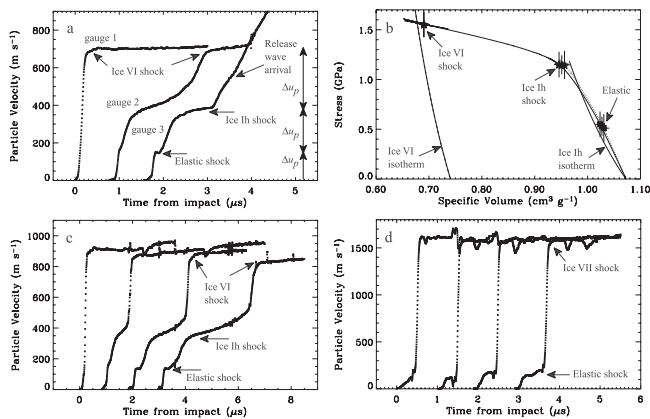
Figure 1. (a) Particle velocity vs. time gauge records measured at 3-mm intervals within ice target subject to 1111 m s^{-1} impact with polycarbonate producing 3-wave shock front. (b) Shock loading σ-V path (corresponding to a) indicating intermediate states at 0.53 and 1.15 GPa and final shock state at 1.55 GPa. (c) Records from 1473 m s^{-1} impact to 2.1 GPa. (d) Records from 2618 m s^{-1} impact to 5.2 GPa.

front. The new data for dynamic yielding at 100 K indicate that HEL states plot metastably in the ice II field at principal stresses up to 0.6 GPa (pressures up to 0.4 GPa), clearly unrelated to melting. The additional dependence on peak pressure (proportional to strain rate in the shock front [*Miller and Ahrens*, 1991]) is consistent with the onset of brittle failure.

[6] The second wave in Figures 1a and 1b at u_p = 370 m s^{-1} (1.15 GPa) corresponds to a shock state in ice Ih, and the final shock wave, at 695 m s^{-1} (1.55 GPa), deforms ice Ih into the ice VI structure (region 3, Figure 3). Identification of the high-pressure phase is made by comparison between its full pressure-volume-temperature static equation of state (EOS) and the shock state (100 K isothermal compression curves [*Petrenko and Whitworth*, 1999] shown for clarity in Figure 1b). A similar three-wave phenomenon is recorded in an experiment with peak pressure of 2.1 GPa (Figure 1c), with an elastic shock at 145 m s^{-1} and 0.525 GPa, a transition ice Ih deformation shock at 360 m s^{-1} and 1.16 GPa, and a final shock state at 883 m s^{-1} and 2.1 GPa, also in excellent agreement with the EOS of ice VI.

[7] At shock pressures above 2.2 GPa, particle velocity profiles (e.g., Figure 1d) indicate a two wave front structure composed of an elastic shock (160 m s^{-1}, 0.56 GPa) and transformation shock. The ~1.15 GPa ice Ih transition shock (e.g., Figures 1a and 1c) is overdriven by a transformation shock wave (1600 m s^{-1}, 5.2 GPa) into the ice VII structure (region 4, Figure 3). The next higher pressure shock datum for ice initially at 263 K, at 7 GPa from *Bakanova et al.* [1976], indicates a sudden *increase* in specific volume along the Hugoniot, signaling a transition to the regime where liquid water is present in the shock state (region 5, Figure 3). At shock pressures >5.5 GPa, direct shock transformation to liquid water overdrives the elastic shock, resulting in a single wave shock front.

4. Discussion

[8] The present and previously published data are combined to derive the first complete definition of the H$_2$O ice

Hugoniot, covering the range of available data (up to 51 GPa), and valid between 100 to 263 K (Table 1). In the multiple-wave region <6 GPa, we include only the published data that (1) resolve each wave in the shock front to account for the elastic precursor and (2) record steady shock waves in order to derive Hugoniot states. We include all published points >6 GPa.

[9] The Hugoniot is expressed as linear fits between shock velocity, U_S, and the jump in particle velocity, Δu_p, for each wave in the shock front (e.g., Figure 1a). These data may be transformed from $U_S - u_p$ to pressure-volume via the Rankine-Hugoniot (RH) equations [*Rice et al.*, 1958]. From the use of Δu_p rather than the more common absolute particle velocity, a single set of equations may be used to define both the 100 and 263 K Hugoniots. The Hugoniots are constructed in segments corresponding to each type of shock wave: elastic shock, ice Ih shock, and transformation shocks to ice VI, VII, and liquid. The RH equations are applied using the initial zero-pressure state for the first, elastic shock region. Then, the mean elastic shock state is used as the initial condition for the RH equations to describe the second region, and so on. The differences between the 100 and 263 K Hugoniots (solid and dashed lines, Figure 3b) arise from: (1) the initial volume dependence on temperature; (2) the magnitude of the mean elastic shock, σ_E; (3) the presence of an ice Ih transition shock preceding the ice VI transformation shock on the 100 K curve (three-wave shock profile). Parameterization with Δu_p removes the temperature-dependent elastic and ice Ih transition shocks from the equations describing transformation shocks to ices VI and VII.

[10] The properties of the three-wave shock front in ice Ih are very unusual and exhibit path and temperature-dependent behavior. On the 100 K Hugoniot, the ice Ih transition shock has an upper limit, or cusp, at 1.15 GPa, before transformation to ice VI, similar to the α-iron cusp at 13 GPa before transformation to the ε phase [*Minshall*, 1955]. The SiO$_2$ Hugoniot may have a similar cusp near 23 GPa, between the α-quartz to stishovite phase transformation
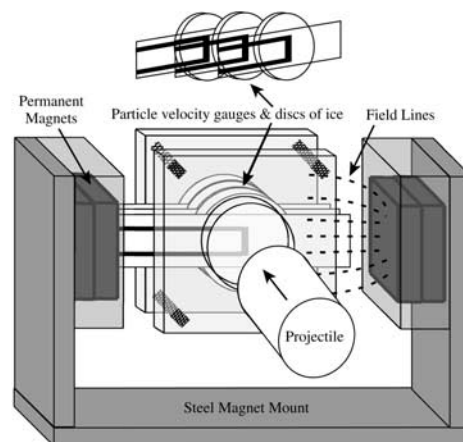

Figure 2. Sketch of particle-velocity gauge method for measuring Hugoniot states in 100 K ice. Shock velocities determined from wave arrival time at each gauge. Particle velocity, u_p (m s^{-1}), is calculated from voltage signal, E (volts), using Faraday's law, $u_p = E/(LH)$, gauge length L (m), and magnetic field strength H (Tesla).
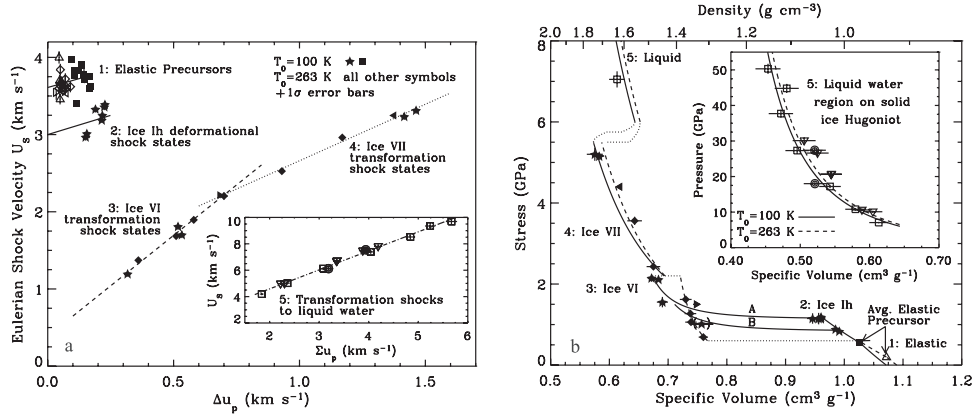
Figure 3. (a) $U_S - \Delta u_p$ fits to combined 100 and 263 K shock data sets: ■★ this work, ▽○ [*Anderson*, 1968], □ [*Bakanova et al.*, 1976], ► [*Gaffney and Smith*, 1994], △✦ [*Larson*, 1984], ◄ [*Davies and Smith*, 1994]. (b) Solid ice Hugoniots centered at 100 K (solid) and 263 K (dashed). Dotted lines connect five well-defined regions along individual Hugoniots.

[*Zhugin et al.*, 1994]. On the 263 K Hugoniot, data records in the same regime [*Larson*, 1984] (dashed line, region 3, Figure 3b) show two-wave shock fronts (elastic shock and ice VI transformation shock) rather than three-wave structures. Furthermore, at both 100 and 263 K, experiments with final shock states just above the elastic limit produce decaying shock waves, which do not define Hugoniot states. Steady ice Ih shocks have only been recorded as transition shocks.

[11] The new 100 K data also exhibits path-dependent shock loading, which is not observed in iron and results in a Hugoniot which is not single-valued in pressure (solid line, region 3, Figure 3b). The "A" locus corresponds to final shock states >1.15 GPa which drive through the ice Ih cusp. The "B" locus is derived from a single experiment, with peak shock stress of 1.015(±.015) GPa shown in parenthesis, which records an ice Ih transition shock state at 0.86 GPa. The final 1.015 GPa shock state appears to be ice VI, rather than ice Ih (as expected if the behavior were similar to other materials with transition shock cusps). We infer that the amplitude of the ice Ih transition shock depends on the final shock pressure and will be variable under conditions which ultimately produce ice VI at pressures between 0.6 and 1.15 GPa. This regime warrants further exploration.

[12] Using the new ice Hugoniot, we derive the critical shock pressures required to initiate and complete melting of ice on planetary surfaces. The shock-induced phase transformation of ice Ih directly to ice VI or ice VII (bypassing the stable phase space for ices II, III, and V) and the corresponding increase in density (Figure 3b) give rise to large increases in entropy leading to shock-melting at surprisingly low pressures. We assume in Figure 4 that entropy increase occurs only via shock-compression and rarefaction occurs isentropically from the Hugoniot state, vertically down to zero pressure. The 100 K Hugoniot curve crosses from ice Ih to the ice VI field above 0.6 GPa, but the entropy increase is almost negligible because of the propor-
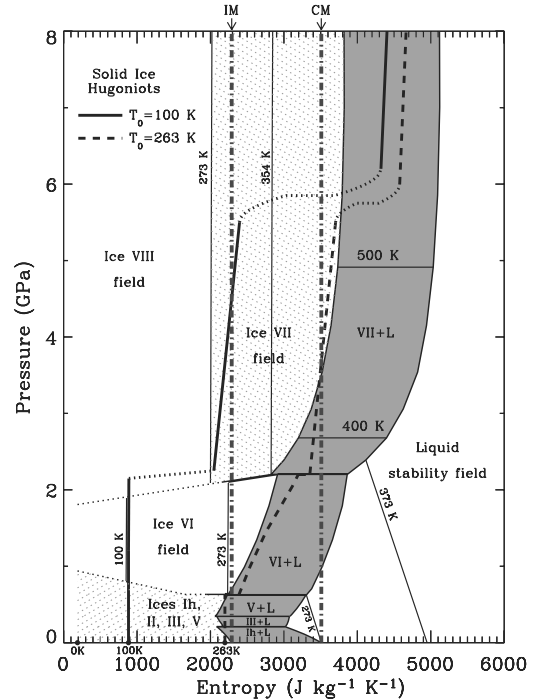
Table 1. $U_S - \Delta u_p$ Shock Equation of State, $U_S = c + s\Delta u_p$, Used to Calculate Ice Hugoniot

Hugoniot Region	c (m s^{-1})	s ...	Δu_p range (ms^{-1}) Min	Max
1. Elastic	3610 (±61)	0.92 (±.63)	0	175
2. Ice Ih	3000 (±100)	1.00 (±.80)	0	230
3. Ice VI	388 (±78)	2.61 (±.14)	100	850
4. Ice VII	1200 (±140)	1.46 (±.11)	600	1540
5. Liquid	1700 (±130)	1.440 (±.035)	1590	...

For 100 K: ρ_0 = 932 kg m^{-3} [*Hobbs*, 1974], σ_E = 0.55 GPa, ice Ih cusp at 1.15 GPa. For 263 K: ρ_0 = 918 kg m^{-3}, σ_E = 0.2 GPa.

Figure 4. 100 and 263 K ice Hugoniots and partial simplified H$_2$O phase diagram in pressure-entropy space [*Bosnjakovic et al.*, 1970; *Dorsey*, 1940; *Fei et al.*, 1993; *Mishima et al.*, 1979; *Petrenko and Whitworth*, 1999]. IM and CM denote critical entropies for incipient and complete melting upon release to zero pressure. Both Hugoniots exit the ice VII-liquid boundary and enter the liquid field around 20 GPa (off plotted pressure range).

tionally large amplitudes of the elastic and ice Ih transition shocks (e.g., Figure 1b). Shock transformation to ice VII, above 2.2 GPa, results in a large (>1100 J kg^{-1} K^{-1}) entropy increase. Above 4.5 GPa, sufficient entropy is produced (2300 J kg^{-1} K^{-1}), that upon isentropic release, incipient melting (IM) occurs. The entropy for complete melting (CM, 3500 J kg^{-1} K^{-1}) upon release requires shock pressures >5.5 GPa. On the 263 K Hugoniot, the elastic compression region appears to metastably bypass the ice Ih + L, ice III + L, and ice V + L fields. The onset of transformation to ice VI begins at 0.6 GPa, where the entropy required for IM is achieved, and a shock pressure of 3.7 GPa provides sufficient entropy for CM. Previous estimates of the critical shock pressures for melting in ice were two to five times higher [*Ahrens and O'Keefe*, 1985; *Kieffer and Simonds*, 1980] or limited to 263 K ice [*Pierazzo et al.*, 1997].

5. Conclusions

[13]   The new criteria for shock-induced melting of water ice have broad application in the solar system. Widespread melting during impact crater formation will soften crater morphologies [*Turtle and Pierazzo*, 2001] and incorporate liquid water into ejecta blankets [*Stewart*, 2002]. *Stewart et al.* [2001] conducted simulations of impact cratering onto ice-silicate mixtures that demonstrate fluidization of ejecta blankets, related to distal scarp structures called ramparts. Rampart crater morphologies, found in great abundance on Mars [*Carr et al.*, 1977], are also seen on the icy surfaces of Europa [*Moore et al.*, 1998; *Turtle and Pierazzo*, 2001] and Ganymede [*Horner and Greeley*, 1982]. The new H₂O Hugoniot shows that the pressures required for shock-induced melting during impact cratering upon the cold icy satellites of the outer solar system are even lower than previously assumed. These results also have implications for collisional processing of cometesimals before ejection into the Oort cloud [*Stern and Weissman*, 2001] (mutual impact velocities of 100's m s^{-1}) and within the Kuiper belt [*Durda and Stern*, 2000] (present mutual collisions at ~1000 m s^{-1}). Although collisions between pure ice at crystal density would not suffer shock-induced melting at these velocities, cometary objects, expected to be mixtures of ice, organic, and silicate materials with 30–80% porosity will readily undergo partial melting. Hence, we infer that cometesimals in the Oort cloud and Kuiper belt have experienced thermal and chemical processing through partial melting during collisional evolution.

References

Ahrens, T. J., Shock wave techniques for geophysics and planetary physics, in *Methods of Experimental Physics*, edited by C. G. Sammis and T. L. Henyey, pp. 185–235, 1987.

Ahrens, T. J., and J. D. O'Keefe, Shock vaporization and the accretion of the icy satellites of Jupiter and Saturn, in *Ices in the Solar System*, edited by J. Klinger et al., pp. 631–654, Kluwer Acad., Norwell, Mass., 1985.

Anderson, G. D., The equation of state of ice and composite frozen soil material, *Res. Rep. 257*, Cold Reg. Res. and Eng. Lab., Hanover, N. H., 1968.

Bakanova, A. A., et al., Thermodynamic properties of water at high pressures and temperatures, *Sov. Phys. JETP, Engl. Transl.*, 41, 544–548, 1976.

Bosnjakovic, F., U. Renz, and P. Burow, *Mollier Enthalpy, Entropy-Diagram for Water, Steam and Ice*, Taylor and Francis, Philadelphia, Pa., 1970.

Carr, M. H., et al., Martian impact craters and emplacement of the ejecta by surface flow, *J. Geophys. Res.*, 82, 4055–4065, 1977.

Davies, F. W., and E. A. Smith, High pressure equation of state investigation of rocks, *Tech. Rep. DNA-TR-94-1*, Def. Nucl. Agency, Washington, D. C., 1994.

Dorsey, N. E., *Properties of Ordinary Water-Substance*, Reinhold, New York, 1940.

Durda, D. D., and S. A. Stern, Collision rates in the present-day Kuiper Belt and Centaur regions: Applications to surface activation and modification on comets, Kuiper Belt objects, Centaurs, and Pluto-Charon, *Icarus*, 145, 220–229, 2000.

Fei, Y., H.-K. Mao, and R. J. Hemley, Thermal expansivity, bulk modulus, and melting curve of H₂O-ice VII to 20 GPa, *J. Chem. Phys.*, 99, 5369–5373, 1993.

Fowles, R., and R. F. Williams, Plane stress wave propagation in solids, *J. Appl. Phys.*, 41, 360–363, 1970.

Gaffney, E. S., Hugoniot of water ice, in *Ices in the Solar System*, edited by J. Klinger et al., pp. 119–148, Kluwer Acad., Norwell, Mass., 1985.

Gaffney, E. S., and E. A. Smith, HYDROPLUS experimental study of dry, saturated, and frozen geological materials, *Tech. Rep. DNA-TR-93-74*, Def. Nucl. Agency, Washington, D. C., 1994.

Hobbs, P. V., *Ice Physics*, Oxford Univ. Press, New York, 1974.

Horner, V. M., and R. Greeley, Pedestal craters on Ganymede, *Icarus*, 51, 549–562, 1982.

Kieffer, S. W., and C. H. Simonds, The role of volatiles and lithology in the impact cratering process, *Rev. Geophys.*, 18, 143–181, 1980.

Larson, D. B., Shock-wave studies of ice under uniaxial strain conditions, *J. Glaciol.*, 30, 235–240, 1984.

Marsh, S. P., *LASL Shock Hugoniot Data*, Univ. of Calif. Press, Berkeley, 1980.

Miller, G. H., and T. J. Ahrens, Shock-wave viscosity measurement, *Rev. Mod. Phys.*, 63, 919–948, 1991.

Minshall, S., Investigation of a polymorphic transition in iron at 130 k.b., *Phys. Rev.*, 98, 271, 1955.

Mishima, O., N. Mori, and S. Endo, Thermal expansion anomaly of ice VI related to the order-disorder transition, *J. Chem. Phys.*, 70, 2037–2038, 1979.

Moore, J. M., et al., Large impact features on Europa: Results of the Galileo nominal mission, *Icarus*, 135, 127–145, 1998.

Petrenko, V. F., and R. W. Whitworth, *Physics of Ice*, Oxford Univ. Press, New York, 1999.

Pierazzo, E., A. M. Vickery, and H. J. Melosh, A reevaluation of impact melt production, *Icarus*, 127, 408–423, 1997.

Rice, M. H., R. G. McQueen, and J. M. Walsh, Compression of solids by strong shock waves, *Solid State Phys.*, 6, 1–63, 1958.

Stern, S. A., and P. R. Weissman, Rapid collisional evolution of comets during the formation of the Oort cloud, *Nature*, 409, 589–591, 2001.

Stewart, S. T., Collisional processes involving icy bodies in the solar system, Ph.D. thesis, Calif. Inst. of Technol., Pasadena, 2002.

Stewart, S. T., J. D. O'Keefe, and T. J. Ahrens, The relationship between rampart crater morphologies and the amount of subsurface ice (abstract), *Proc. Lunar Planet. Sci. Conf. 32nd*, 2092, 2001.

Turtle, E. P., and E. Pierazzo, Thickness of a Europan ice shell from impact crater simulations, *Science*, 294, 1326–1328, 2001.

Zhugin, Y. N., et al., On some peculiarities of dynamic compressibility of quartz, *Phys. Solid Earth*, 30, 868–874, 1994.

———————————

S. T. Stewart and T. J. Ahrens, Lindhurst Laboratory of Experimental Geophysics, 252-21, California Institute of Technology, Pasadena, CA 91125, USA. (tja@caltech.edu)

S. T. Stewart, Geophysical Laboratory, Carnegie Institution of Washington, 5251 Broad Branch Road, N.W., Washington, D. C. 20015, USA. (sstewart@gl.ciw.edu)